Received: 24 March 2020 | Revised: 18 June 2020 | Accepted: 22 June 2020 | Published online: 22 August 2020

DOI: 10.1002/dad2.12068

Alzheimer's & Dementia
Diagnosis, Assessment & Disease Monitoring

RESEARCH ARTICLE

Anterolateral entorhinal cortex thickness as a new biomarker for early detection of Alzheimer's disease

Andrew J. Holbrook[1] | **Nicholas J. Tustison**[2,3] | **Freddie Marquez**[3] | **Jared Roberts**[3] | **Michael A. Yassa**[3] | **Daniel L. Gillen**[4] | **for the Alzheimer's Disease Neuroimaging Initiative**[§]

[1] Department of Biostatistics, University of California, Los Angeles, California, USA

[2] Department of Radiology and Medical Imaging, University of Virginia, Charlottesville, Virginia, USA

[3] Department of Neurobiology and Behavior and Center for the Neurobiology of Learning and Memory, University of California, Irvine, Irvine, California, USA

[4] Department of Statistics, University of California, Irvine, California, USA

Correspondence
Andrew Holbrook, Department of Biostatistics, University of California, Los Angeles, CA, USA.
Email: aholbroo@g.ucla.edu
Daniel Gillen, Department of Statistics, University of California, Irvine, CA, USA.
Email: dgillen@uci.edu
Michael Yassa, Department of Neurobiology and Behavior and Center for the Neurobiology of Learning and Memory, University of California, Irvine, Irvine, CA, USA.
Email: myassa@uci.edu

[§] Data used in preparation of this article were obtained from the Alzheimer's Disease Neuroimaging Initiative (ADNI) database (http://adni.loni.usc.edu). As such, the investigators within the ADNI contributed to the design and implementation of ADNI and/or provided data but did not participate in analysis or writing of this report. A complete listing of ADNI investigators can be found at: http://adni.loni.usc.edu/wp-content/uploads/how_to_apply/ADNI_Acknowledgement_List.pdf.

Funding information
NSF, Grant/Award Numbers: DGE-1321846, B2D-1612490; NIA, Grant/Award Numbers: R01AG053555, P50AG05146; Alzheimer's Disease Neuroimaging Initiative; National Institutes of Health, Grant/Award Number: U01 AG024904; DOD; ADNI, Grant/Award Number: W81XWH-12-2-0012; National Institute on Aging; National Institute of Biomedical Imaging and Bioengineering

Abstract

Introduction: Loss of entorhinal cortex (EC) layer II neurons represents the earliest Alzheimer's disease (AD) lesion in the brain. Research suggests differing functional roles between two EC subregions, the anterolateral EC (aLEC) and the posteromedial EC (pMEC).

Methods: We use joint label fusion to obtain aLEC and pMEC cortical thickness measurements from serial magnetic resonance imaging scans of 775 ADNI-1 participants (219 healthy; 380 mild cognitive impairment; 176 AD) and use linear mixed-effects models to analyze longitudinal associations among cortical thickness, disease status, and cognitive measures.

Results: Group status is reliably predicted by aLEC thickness, which also exhibits greater associations with cognitive outcomes than does pMEC thickness. Change in aLEC thickness is also associated with cerebrospinal fluid amyloid and tau levels.

Discussion: Thinning of aLEC is a sensitive structural biomarker that changes over short durations in the course of AD and tracks disease severity—it is a strong candidate biomarker for detection of early AD.

KEYWORDS
ADNI-1, Alzheimer's disease, anterolateral entorhinal cortex, biomarker, brain imaging, Clinical Dementia Rating, cortical thickness, cerebrospinal fluid amyloid, linear mixed-effects models, memory, mild cognitive impairment, Mini-Mental State Exam, posteromedial entorhinal cortex, receiver operating characteristic

1 | INTRODUCTION

Layer II of the entorhinal cortex (EC) is one of the earliest sites for the accumulation of tangle pathology and neurodegeneration in the course of Alzheimer's disease (AD).[1-3] Quantitative studies of neuron numbers in autopsy brains characterized for AD pathology have shown that a substantial reduction in EC is observed by the time of dementia diagnosis and further progressive loss of EC neurons occurs over the course of the disease.[4-6] Little or no neuron loss occurs within EC in healthy aged brains without AD pathology suggesting that EC neurodegeneration is specific to disease.[4]

Histopathological data indicate that the transentorhinal region, which consists of the anterolateral EC (aLEC) and perirhinal cortex, is vulnerable in the early stages of AD (Braak stages I and II[2]). Recent evidence has elucidated a functional subdivision in the EC whereby the lateral and medial portions are involved in different aspects of information processing[7] and are differentially connected with the perirhinal and parahippocampal cortices.[8] Other work has shown that the aLEC (which maps onto the lateral EC in rodents) is selectively vulnerable to age-related alterations in processing[9] as well as structural changes associated with age-related cognitive decline[10] in contrast to the posteromedial portion (pMEC). While volume reductions in the EC independently predict the likelihood of conversion from healthy aging to amnestic mild cognitive impairment (MCI) and from MCI to AD,[11-13] preceding and predicting hippocampal volume reduction,[14] it is unclear whether these volumetric changes are primarily driven by the aLEC or the pMEC.

Given the need for improved diagnostic biomarkers that are capable of detecting the earliest signs of neurodegeneration and the wealth of evidence pointing to the EC as an early site of structural decline, we seek to determine whether we can identify different trajectories of structural thinning in the aLEC and pMEC in healthy, MCI, and AD individuals.

The Alzheimer's Disease Neuroimaging Initiative (ADNI[15]) began in 2003 with the goal of developing imaging, genetic, and pathological biomarkers for early detection and longitudinal progression in AD. This multisite imaging endeavor provides investigators with open access to serial magnetic resonance imaging (MRI) scans from nondemented individuals as well as MCI and AD patients, in conjunction with other biomarker data such as cerebrospinal fluid (CSF) amyloid and tau pathological markers. Measurements of cortical thickness (CT) have recently emerged as potential candidates for biomarkers due to their superior sensitivity to layer-specific cortical atrophy compared to volumetric approaches and the availability of automated methods for estimation.[16] In the ADNI sample, EC CT was the most powerful measure of structural change both in MCI and AD brains.[17] EC thinning also preceded and predicted hippocampal atrophy[18] and predicted conversion to AD with the greatest accuracy.[19]

For EC thinning to be a reliable and robust measurement that accurately reflects neurodegeneration and supports longitudinal tracking of disease progression, several common methodological limitations need to be addressed.[20] These issues include registration bias and inverse consistency, bias due to asymmetric interpolation favoring the baseline scan in longitudinal pipelines,[21] and susceptibility to errors in segmentation or overestimation of gray matter thickness without specified anatomical constraints.[22]

Here, we apply a novel pipeline that we recently developed for longitudinal registration-based CT to quantify aLEC and pMEC thinning that directly addresses these pitfalls and extend prior findings that EC thickness reliably differentiates normal controls from MCI patients and MCI patients from AD patients in the ADNI sample. Using linear mixed-effects (LME) models, we quantify cross-sectional and longitudinal associations between aLEC and pMEC thickness and two cognitive outcomes, the Clinical Dementia Rating–Memory box score (CDRM) and the Mini-Mental State Exam (MMSE), while controlling for possible confounding variables including age, sex, total brain volume and apolipoprotein E (*APOE*) $\varepsilon 4$ genotype. We supplement this analysis of cognitive outcomes by using further LME models to establish diagnostic cohort specific trajectories in aLEC and pMEC CT through time and receiver operating characteristic (ROC) curves to ascertain predictive value of raw aLEC and pMEC CT for diagnostic outcomes. In a secondary analysis, we use an LME model to follow trajectories in aLEC and pMEC CT through time for two subcohorts with differing CSF amyloid profiles.

RESEARCH IN CONTEXT

1. **Systematic review**: The authors reviewed the literature using Pubmed. While there is substantial evidence that the entorhinal cortex is the site of early tau pathology, little is known about how components of the entorhinal cortex (EC) longitudinally change in mild cognitive impairment and Alzheimer's disease (AD). Specifically, the anterolateral EC (aLEC) may be more vulnerable than the posteromedial EC to age-related cognitive decline.
2. **Interpretation**: Our findings suggest that aLEC thinning is associated with cognitive decline as well as amyloid and tau pathologies.
3. **Future directions**: This work posits that aLEC thinning is a potential biomarker for preclinical AD. Further work will be needed to (1) determine aLEC's utility as an outcome measure for clinical trials, (2) develop and refine cognitive assessments that are maximally sensitive and specific to aLEC, (3) determine how aLEC thinning may contribute to subsequent decline, and (4) determine whether slowing this thinning can provide disease modification.

2 | MATERIALS AND METHODS

2.1 | Raw imaging data and preprocessing

All T1-weighted MPRAGE MRI scans used in this study were drawn from the publicly available ADNI. Exact parameters for the sequences acquired are available on http://adni.loni.usc.edu. Due to limited contrast between EC regions and surrounding areas in T1-weighted MRI, we use the multi-atlas joint label fusion methodology[23] for EC parcellation and subsequent thickness estimation based on combined T1- and T2-weighted image information from a set of gold-standard atlases (see below), permitting a more robust weighted consensus approach than single-template and/or T1-weighted-only alternatives.

2.2 | Atlas data

We use a set of 17 atlases for multi-atlas joint label fusion comprising T1/T2-weighted image pairs and corresponding segmentation labels for the following left/right regions (aLEC, pMEC, perirhinal cortex, parahippocampal cortex, DG/CA3, CA1, and subiculum). Manual atlas labeling uses the T2-weighted image for each atlas set and a well-established and validated protocol.[9] Atlas labels for a single subject are shown in Figure S1 in supporting information superimposed on the corresponding T2-weighted image. The scans used to compose the atlases were collected on a Philips 3T scanner at the University of California, Irvine. T1-weighted MPRAGE scans were acquired in the sagittal orientation with an isotropic image resolution of $0.75 \times 0.75 \times 0.75$ mm^3. Image acquisition for the T2-weighted protocol was angled perpendicular to the long axis of the hippocampus consistent with previous work.[24] T2-weighted image resolution is $0.47 \times 0.47 \times 2.0$ mm^3. The optimal rigid transformation between each individual atlas' T1- and T2-weighted images was determined using the Advanced Normalization Tools (ANTs) software package.[25,26]

2.3 | Population-specific templates

To facilitate aLEC/pMEC thickness estimation for the ADNI cohort described below, two population-specific, optimal shape/intensity templates were generated. The first T1-weighted template was constructed from 52 cognitively normal ADNI-1 subjects for a separate ADNI-based investigation,[27] and we opted to use it in this study because it provides an intermediate registration space for transforming the labels of the 17 atlases. The second T1-weighted template, the "UCI" template, was generated from the 17 T1-weighted atlas images discussed above.[28] Representative slices for both templates are shown in Figure S2 in supporting information. ANTs-based symmetric normalization (SyN) was used to determine optimal diffeomorphic transformation between the two T1-weighted templates. This permits the two T1-weighted templates to act as an intermediate geometric space for the "pseudo-geodesic" mapping[29] between a set of atlas labels and the individual T1-weighted time point.

2.4 | Individual time point processing

Processing was conducted using the recently developed ANTs longitudinal structural processing pipeline,[27] which is an extension of the previously reported cross-sectional framework.[30] Briefly, the T1-weighted images constituting the set of subject's longitudinal data were used to create a single-subject template (SST) as an unbiased space for processing longitudinal time points of individual subjects.[21] The SST was then processed through the cross-sectional pipeline using the ADNI-1 template mentioned earlier. This processing produced the SST auxiliary images (ie, *n*-tissue segmentation priors and brain extraction mask prior) used for individual time point brain extraction and tissue segmentation into CSF, cortical gray matter, white matter, deep gray matter, brain stem, and cerebellum. Output of this processing stream includes the transforms between the individual time point and the SST and the transforms between the SST and the ADNI-1 template. In this way, concatenation of transforms can be used to map each of the 17 atlas label sets to each individual time point through a set of intermediary spaces which constitutes the "pseudo-geodesic" transform. This strategy has the benefit of reducing diffeomorphic distances between registration image pairs, reducing computational costs in terms of the sheer number of registrations, and taking advantage of the longitudinal nature of the data. This pseudo-geodesic mapping strategy is illustrated in Figure S3 in supporting information.

2.5 | Multi-atlas joint label fusion

After mapping the set of 17 atlas label sets to each individual time point, the multi-atlas joint label fusion[23] approach is applied. This technique weights the contribution of each atlas while minimizing informational redundancy between the atlases. To estimate CT for each EC region, we base our strategy on the MindBoggle approach[31] but, instead of using a mesh-based surface area calculation, we opt for the more accurate Crofton's formula,[32] which estimates the surface area directly.

2.6 | Statistical analyses

Our primary interest is the linear association between cognitive performance (CDRM and MMSE), diagnostic status (healthy, MCI, and AD) and CT in the aLEC and pMEC. We seek to discern whether declining cognitive performance tracks with deterioration of CT within the two subregions. We also ask whether clinical diagnostic groups are separable when viewed through subregion CTs and their trajectories through time.

LME[33] modeling allows us to leverage the longitudinal nature of the ADNI repeated-measures design insofar as a correctly specified LME model adjusts for within-subject correlation structure through time. As an extension of the multiple linear regression framework, LME modeling also supports adjustment for possible confounding variables as well as inclusion of precision variables. For the primary analysis, we use three LME models in total, each of which features subject-specific random intercepts and slopes through time. We decide on the inclusion of random components using the modified likelihood ratio test.[34]

With the first two models we wish to understand cognitive performance as a linear function of CT and its change through time. Both of these models regress either CDRM or MMSE over aLEC or pMEC CTs (and functions thereof) independently. We fit each model once for aLEC thickness as predictor of interest and once for pMEC thickness as predictor of interest because simultaneous inclusion of both measures results in multicollinearity on account of correlations between subregional CT. The first model evaluates cognitive score as a function of baseline thickness and the interaction between baseline thickness and months since baseline. The second model evaluates cognitive score as a function of baseline thickness and loss of thickness through time. We stratify the first two models by diagnostic cohort due to the possibility of diagnosis-based non-linearities in associations through time. Stratification decreases statistical power but increases model robustness.

Another primary question is whether population CT averages and their trajectories through time can be separated as a function of healthy, MCI, and AD statuses. A third LME model (Model 3) independently regresses aLEC or pMEC CTs over diagnostic status and its interaction with months from baseline. We supplement Model 3's inferential analysis with ROC curves[35] and area under these curves (AUC) to demonstrate prediction of diagnostic statuses using aLEC or pMEC thicknesses alone. We compare these AUCs to that of hippocampal volume and use the nonparametric bootstrap to obtain confidence intervals for the differences between AUCs.

Given positive results, we motivate future research by asking the secondary question whether differential associations between CSF amyloid levels and aLEC/pMEC CTs provides explanatory power for primary analysis results. Based on prior work,[36-39] Model 4 considers the ratio between p-tau and amyloid beta (Aß) binarized at the threshold 0.1 as predictor for CT in aLEC and pMEC subregions. All models are outlined in Table 1. All modeling decisions were made prior to data access.

We use the R programming language[40] for all statistical analyses. We use the nlme package[41] for LME model fitting, the ggplot2 package[42] for visualization, the plotROC package for generating ROC curves,[43] and the boot package for bootstrap confidence intervals. For exploratory analyses, we: present a data table with means, proportions, and standard deviations of outcomes and model covariates stratified by diagnostic cohort; plot aLEC and pMEC thicknesses as a function of subject age, stratifying by sex; and use nearest neighbor misclassification as an index of homogeneity.

3 | RESULTS

3.1 | Data distributions

We provide descriptive statistics for outcomes, predictors, and other covariates in Table 1 organized by diagnostic cohort. For each cohort, means and standard deviations appear for continuous variables and level-wise percent membership appears for factors.

For both baseline aLEC and baseline pMEC CT, the controls have the highest values, the AD cohort has the least, and the MCI cohort is in the middle. This trend holds for the longitudinal change in thickness. The AD cohort has the largest percent loss per year, and the MCI cohort has less percent loss per year. For both of these groups the %/yr loss is less for pMEC than it is for aLEC. MMSE and CDRM also follow the cohort-wise trends: baseline MMSE decreases from control cohort to AD cohort and baseline CDRM rises. For both MCI and AD cohorts, CDRM changes more through time than does MMSE.

Figure 1 shows a scatterplot of unadjusted CT and age across sex and diagnostic cohort (healthy control and AD). Figures 1A and C shows aLEC thickness in males and females, respectively, while Figures 1B and D shows pMEC thickness in males and females, respectively. Visibly, there is greater overlap between healthy and AD cohort point clouds as a function of pMEC than as a function of aLEC. We quantify this overlap using the nearest neighbor misclassification rate as a homogeneity index. Regardless of sex, cohort clusters exhibit roughly 70% less homogeneity when viewed with aLEC thickness than with pMEC thickness.

3.2 | EC CT and cognitive performance

Models 1 and 2 regress cognitive performance over baseline and longitudinal CT. Figure 2A contains results from analyses based on Models 1 and 2. Green cells are nominally statistically significant at a 95% confidence level. Baseline CT and percent loss are standardized within cohort to facilitate cross-cohort comparisons and comparisons between the aLEC and the pMEC. In general, aLEC thickness is more predictive of outcome than is pMEC thickness. Across both outcomes (MMSE and CDRM), aLEC thickness has eight significant associations with outcome, whereas pMEC only has three significant associations. In 9 of 12 of the comparisons shown in the table effect sizes are larger for aLEC thickness.

Figure 2 also illustrates Model 2 results but, to facilitate comparisons across CDRM and MMSE and aLEC and pMEC thicknesses, axes are standardized. MCI cohort results are shown in Figure 2B; AD cohort results are shown in Figure 2C. We flipped the sign of MMSE so that lower scores reflect better testing performance for both cognitive measures. In general, regression coefficients reflecting the associations between CDRM or MMSE and aLEC (orange) thickness (and changes thereof) are more significantly non-zero than those of pMEC (blue) thickness. The scaled coefficients of aLEC are uniformly higher than pMEC except for the case of MMSE as a function of % loss CT for

TABLE 1 Outcomes, predictors, and confounding variables

	Control [219]	MCI [380]	AD [176]
Baseline aLEC (mm)	2.19 (0.14)	2.11 (0.20)	1.97 (0.19)
Loss aLEC (%/year)	0.07 (2.59)	1.14 (3.08)	1.34 (4.04)
Baseline pMEC (mm)	1.89 (0.13)	1.85 (0.15)	1.77 (0.16)
Loss pMEC (%/year)	0.14 (2.20)	0.52 (2.40)	0.69 (3.04)
Baseline MMSE	28.00 (1.58)	23.46 (4.89)	22.50 (3.61)
Loss MMSE (%/year)	0.04 (4.79)	2.65 (10.16)	10.06 (17.49)
Baseline CDRM	0.25 (0.35)	0.88 (0.85)	0.17 (0.76)
Gain CDRM (%/year)	N/A	17.12 (53.48)	25.00 (55.54)
Brain volume (CM^3)	1467.21 (138.56)	1499.66 (147.61)	1453.63 (162.10)
Baseline age (years)	75.97 (5.06)	74.93 (7.14)	75.01 (7.63)
APOE (% with (0, 1, 2) ∈4 alleles)	(74, 24, 2)	(47, 42, 12)	(33, 48, 19)
Male (%)	54	64	52

Notes: Continuous variables present as mean (standard deviation). For each continuous variable, we show cohort means and standard deviations. For factors, we show the percentage of the cohort in each level. Baseline variables are shown with their natural scale, whereas change in these variables is shown using percentages to facilitate comparison across variables.
Abbreviations: aLEC, anterior lateral entorhinal cortex thickness; APOE, apolipoprotein 1; CDRM, Clinical Dementia Rating-Memory Score; MMSE, Mini-Mental State Exam Score; pMEC, posterior medial entorhinal cortex thickness.

the AD cohort. For the MCI cohort, both lower baseline aLEC thickness and greater % loss aLEC CT predict worse CDRM and MMSE scores.

Overall, these results indicate that aLEC CT, both at baseline and longitudinally, is more predictive of clinically relevant cognitive changes than pMEC CT. Given the known pathological and neurodegenerative trajectory in the medial temporal lobes, this result is consistent with prior literature and suggests that within the EC, regionally specific cortical thinning measures can be used as a biomarker for cognitive decline.

3.3 | EC CT and clinical diagnosis

Model 3 regresses CT over cohort membership and its interaction with time. In general, estimated effect sizes for aLEC as a function of cohort membership and time are twice those for pMEC. Nonetheless, all linear associations are nominally statistically significant at the 95% confidence level, that is, none of the intervals contain zero.

The top row of Figure 3 illustrates these results as a function of months from baseline. aLEC thickness is regressed over cohort membership and months in Figure 3A; pMEC thickness is regressed over the same in Figure 3B. The three cohorts exhibit greater separation at baseline when viewed through aLEC thickness than they exhibit when viewed through pMEC thickness. Estimated aLEC thickness 95% confidence bands maintain complete separation among cohorts throughout time, whereas estimated pMEC thickness 95% confidence bands do not.

Figure 4 supplements these inferential results with ROC curves to measure predictive content of raw aLEC and pMEC CTs with respect to MCI (Figure 4A) and AD (Figure 4B) status. The aLEC curves are consistently above the pMEC curves and yield higher AUCs, signifying greater predictive content at every threshold of the continuous CT values. Both aLEC and pMEC AUCs outperform those of subject age (MCI 0.47; AD 0.48) and total brain volume (MCI 0.47; AD 0.57).

3.4 | EC CT and CSF AD pathology

Given the stronger associations between aLEC CT and clinical outcomes than between pMEC thickness and the same, we ask whether a stronger link between aLEC thickness and CSF AD pathology levels exists than between pMEC thickness and the same. This secondary analysis provides a basis for future research into physiological mechanisms underlying aLEC CT and its clinical effects.

We look at the longitudinal progressions of aLEC and pMEC thicknesses as a function of the binary threshold given by the ratio of phosphorylated tau-181 (p-tau) to Aß being > 0.1.[36-39] These CSF data are available for a smaller 238 subject (70 healthy; 119 MCI; 49 AD) subset of the data used in the primary analyses. Due to dearth of repeated measures for CSF levels, we consider only the first CSF measurement for each individual and only include CT, CDRM, and MMSE data collected during visits occurring after this CSF measurement with 1-month grace period. Proportions of the ratio of p-tau to Aß that are > 0.1 are 0.9 for the healthy cohort, 0.97 for the MCI cohort, and 1 for the AD cohort. We refer to these subjects as being "p-tau/Aß ratio-positive" or "amyloid ratio-positive."

We model the linear associations between subregion CTs and ratio positivity and its interaction with time from baseline (as measured by time of CSF measurement). The bottom row of Figure 3 presents the estimated linear cross-sectional (Figure 3C) and longitudinal

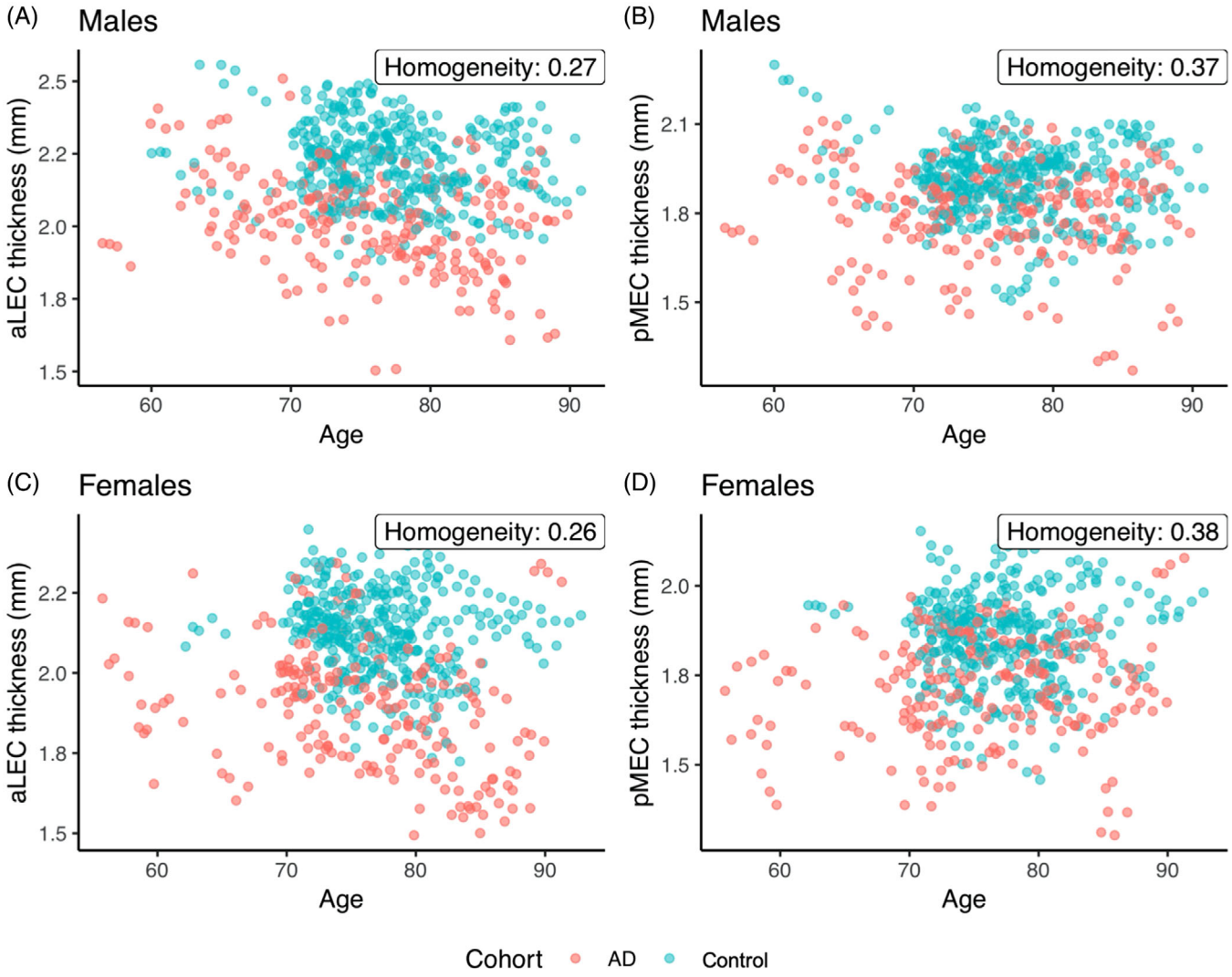

FIGURE 1 Scatterplots featuring anterolateral and posteromedial (anterolateral entorhinal cortex [aLEC] and posteromedial entorhinal cortex [pMEC]) cortical thickness (CT) and age stratified by sex and diagnostic cohort. aLEC thickness in males (A) and females (C) exhibits moderately less overlap between cohorts than does pMEC thickness in males (B) and females (D). We quantify overlap between healthy and Alzheimer's disease (AD) cohorts using nearest neighbor misclassification rate as homogeneity index. For the same comparisons between healthy and mild cognitive impairment cohorts the homogeneity indices read 0.39, 0.43, 0.43, 0.44 from top-left to bottom-right

(Figure 3D) associations along with 95% confidence intervals. Cross-sectionally, we estimate that the population of individuals with amyloid ratio positivity has 0.11 mm less aLEC CT than does the population of individuals who are amyloid ratio negative. For perspective, 0.11 mm is more than the difference between baseline aLEC thickness means of healthy control and MCI cohorts presented in Table 1.

Longitudinally, we estimate that the amyloid ratio-positive sample of individuals experiences an additional loss of 0.025 mm aLEC CT per year compared to the loss experienced by the amyloid ratio-negative sample. The additional loss in aLEC CT experienced by the amyloid ratio-positive sample requires 4 years before the difference between healthy and MCI cohorts is spanned. Due to the smaller sample size in this analysis, the results require further research and should be regarded as preliminary.

3.5 | Benchmarking against hippocampal volume

Finally, to ensure that the predictive validity for MCI and AD status from aLEC CT offers additional information above and beyond hippocampal volume, a well-validated and highly used MRI biomarker, we compared ROC curves for the two structural measures. In Figure S4 in supporting information, total hippocampal volume ties aLEC CT in predicting MCI status with an AUC of 0.69. For prediction of AD status, total hippocampal volume markedly underperforms aLEC CT with an AUC of 0.64 compared to the 0.73 reported above. Overall, these results indicate that relative to hippocampal volume, raw aLEC thickness is a better predictor of AD status and is at least as good a predictor of MCI status. Future research may consider combining aLEC CT with other predictors within a machine learning algorithm to better predict AD onset.

(A)

	Effect	MMSE aLEC	MMSE pMEC	CDRM aLEC	CDRM pMEC
AD	CT_0	0.44 (0.07, 0.82)	0.04 (-0.32, 0.40)	-0.059 (-0.114, -0.005)	-0.030 (-0.083, 0.022)
	CT_0 × months	-0.02 (-0.07, 0.04)	-0.01 (-0.06, 0.04)	-0.001 (-0.006, 0.004)	0.003 (-0.002, 0.008)
	CT Std. % loss	-0.243 (-0.582, 0.097)	-0.332 (-0.655, -0.008)	0.053 (0.014, 0.091)	0.048 (0.006, 0.090)
MCI	CT_0	0.17 (-0.04, 0.39)	-0.02 (-0.23, 0.18)	-0.033 (-0.055, -0.010)	-0.038 (-0.059, -0.017)
	CT_0 × months	0.03 (0.01, 0.05)	0.01 (-0.01, 0.03)	-0.004 (-0.006, -0.002)	-0.001 (-0.003, 0.001)
	CT Std. % loss	-0.210 (-0.374, -0.046)	0.057 (-0.086, 0.200)	0.018 (0.001, 0.036)	0.006 (-0.010, 0.022)

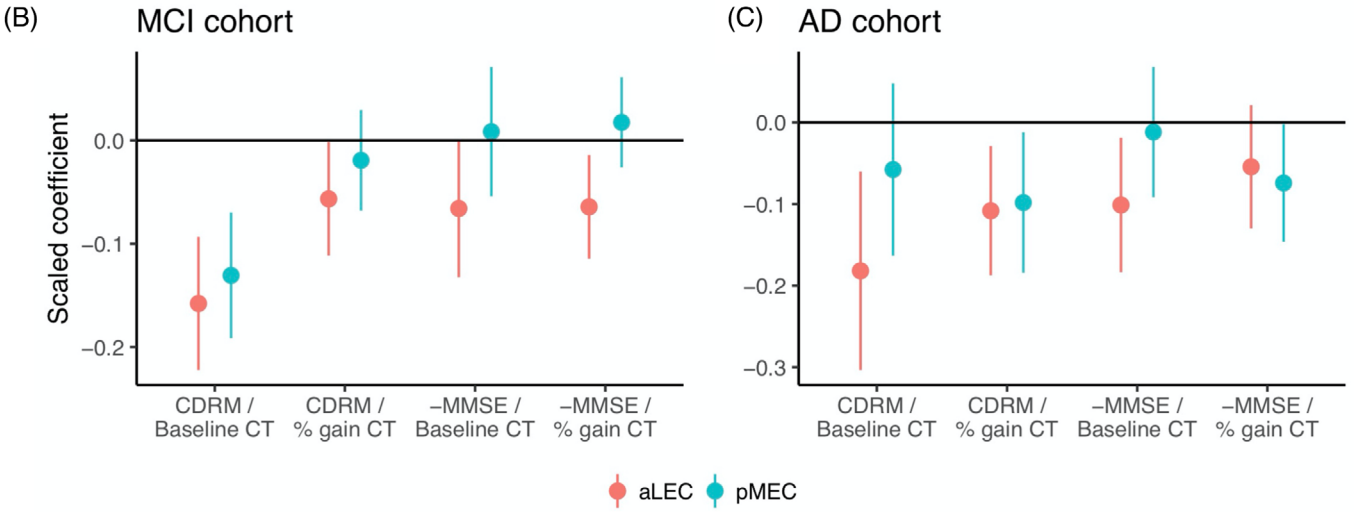

FIGURE 2 Estimated linear associations and nominal 95% confidence intervals between anterolateral and posteromedial entorhinal (anterolateral entorhinal cortex [aLEC] and posteromedial entorhinal cortex [pMEC]) cortical thicknesses (CT) and Mini-Mental State Exam Score (MMSE) or clinical dementia rating-memory score (CDRM). A, For Alzheimer's disease (AD) and mild cognitive impairment (MCI) cohorts, the first row contains cross-sectional associations with baseline thickness (CT_0) whereas the second and third lines contain longitudinal associations. The first, second, and fifth rows belong to Model 1; the third and sixth rows belong to Model 2. Cells for which intervals do not contain zero are green. B–C, Model 2's adjusted linear associations between CDRM or MMSE and aLEC or pMEC baseline thicknesses and percent change in thickness from baseline. Baseline CT, percent gain CT, MMSE, and CDRM are standardized. MMSE is negated since high performance is a higher score for MMSE but lower for CDRM. Associations are stronger for aLEC CT than for pMEC CT for both MCI (B) and AD (C), exhibiting point estimates of greater scale as well as fewer confidence intervals overlapping zero

4 | DISCUSSION

Given the wealth of research implicating the transentorhinal region,[1-3] selective vulnerability of the aLEC to age-related alterations in processing[9] and structural changes associated with age-related cognitive decline,[10] we hypothesized that aLEC structure, specifically CT, might provide a suitable biomarker for early AD detection. We implemented a novel longitudinal CT pipeline on structural MRI data collected from the ADNI-1 cohort and compared this data with MMSE and CDRM performance, diagnostic cohort membership, and CSF amyloid levels. Initial homogeneity analyses showed less overlap between healthy control and AD cohorts as a function of aLEC CT than for pMEC CT. We used LME models to analyze linear associations between these quantities through time while controlling for within-subject correlations and confounders such as age, sex, brain volume, and *APOE* ε4 genotype.

Primary analyses showed statistically and practically significant negative associations between baseline aLEC thickness and progression of cognitive performance over time (Model 1). We also observed statistically and practically significant associations between change in aLEC thickness and cognitive performance through time (Model 2). Cross-sectional and longitudinal correlations between aLEC thickness and cognitive performance were present for both MCI and AD cohorts. We also tested whether trajectories of EC subregional CT through time differentiate by clinical diagnostic grouping (Model 3). aLEC thickness maintained complete separation between 95% confidence bands among healthy, MCI, and AD cohorts while pMEC thickness did not.

Results indicate that the EC subregions could be differentially affected during early stages of AD. This is consistent with histopathological studies, which have reported that neurofibrillary tangles and neuropil threads show a distribution pattern that allow for staging.[3] Initial stages show alterations confined to the transentorhinal region, which includes the aLEC. These results contribute to growing evidence that the aLEC is selectively vulnerable during early AD and also demonstrate that aLEC CT and changes in thickness over time are sensitive to cognitive changes and serve as a viable biomarker for prodromal AD.

In a secondary analysis, we analyzed the relationship between subregional CT and CSF measures of amyloid and tau pathology. Clinical symptoms of AD are preceded by a long preclinical phase in which pathological protein aggregation occurs in the brain.[6,44]

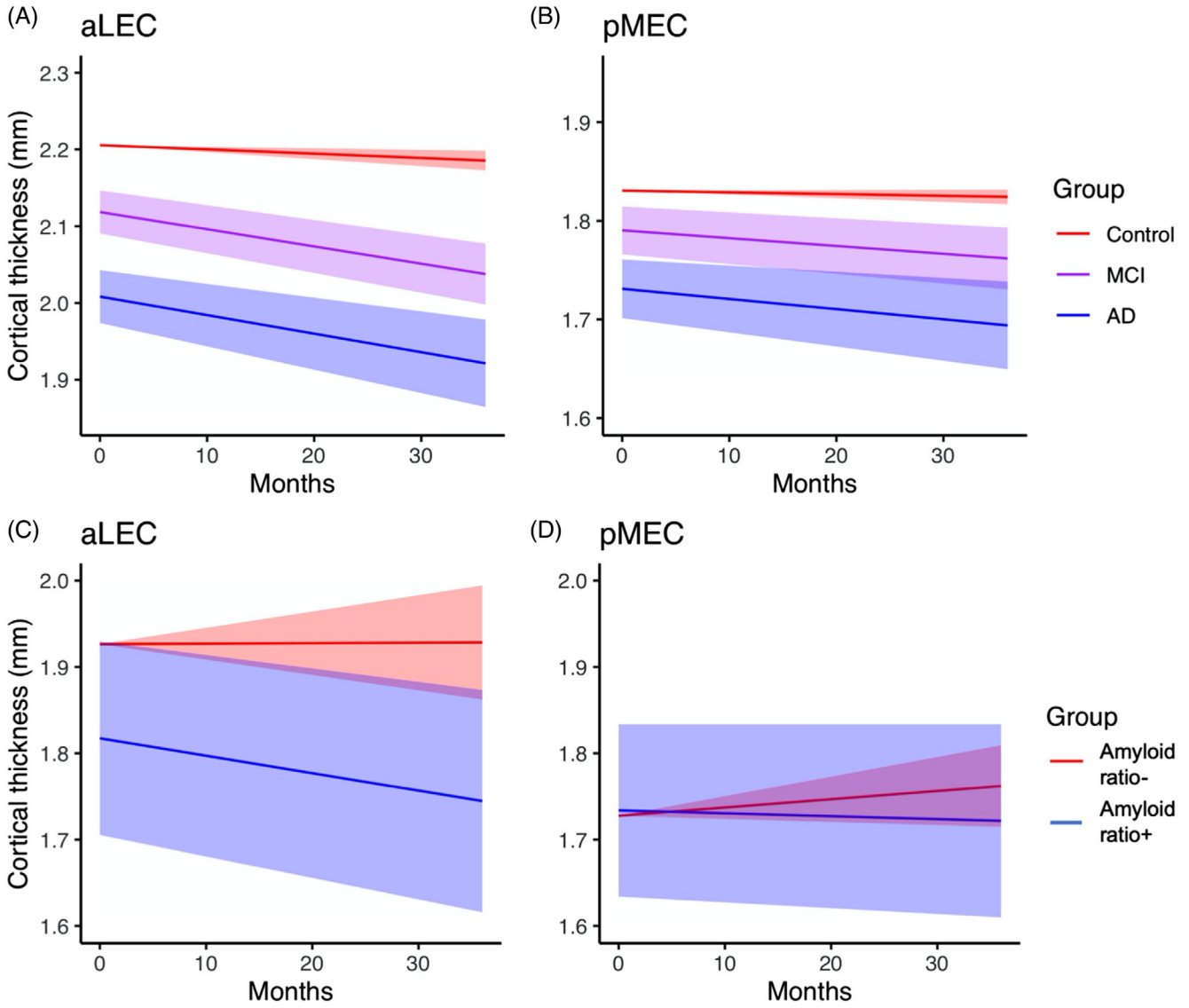

FIGURE 3 Subregion cortical thickness (CT) progressions through time as estimated using Model 3 along with 95% confidence bands. Model 3 accounts for individual variations as well as confounding variables. A–B, When viewed through anterolateral entorhinal cortex (aLEC) CT, the diagnostic cohorts exhibit statistically significant separation that persists through the entire time of measurement. Such separation is not apparent in posteromedial entorhinal cortex (pMEC) CT. C–D, Secondary analysis on subset of Alzhiemer's Disease Neuroimaging Initiative (ADNI-1) cohort comparing progressions for amyloid ratio-positive (p-tau/Aß >0.1) and ratio-negative cohorts shows qualitatively different behavior between aLEC and pMEC CT, suggesting a possible role for cerebrospinal fluid amyloid ratio in influencing aLEC but not pMEC CT trajectory

Additionally, Aβ plaques develop ~15 to 20 years before onset of cognitive impairment and neurofibrillary tangles begin to accumulate at least 5 years before symptom onset.[44] Previous studies have shown low CSF levels of Aβ strongly correlate with increased plaque load in the brain, and that high concentrations of CSF p-tau correlate with AD-specific neurofibrillary pathology.[45,46] Furthermore, ptau$_{181}$–Aβ_{42} ratio (ptau$_{181}$/Aβ_{42}) has been shown to be a strong predictor of conversion from cognitively normal to MCI over an approximately 3- to 4-year period.[36-38]

We found statistically and practically significant linear associations between the binarized ratio p-tau/Aβ >0.1 and aLEC CT and estimated that there are similar differences in aLEC CT levels comparing the p-tau/Aβ ratio-positive sample to the ratio-negative sample as for the comparison between the MCI cohort and the healthy cohort. Furthermore, the p-tau/Aβ ratio-positive sample exhibits a statistically and practically significant change in aLEC thickness over time, requiring an estimated 4 years to span the gap between healthy and MCI cohorts. This secondary analysis suggests the presence of AD-specific neuropathology may mediate thinning of the aLEC over time, but results require further investigation.

Overall, these results suggest that aLEC CT is a sensitive measure to cognitive decline as well as to AD pathological stage. Considering the growing interest in surrogate biomarkers that are sensitive and specific to AD especially during the early stages, we suggest that aLEC

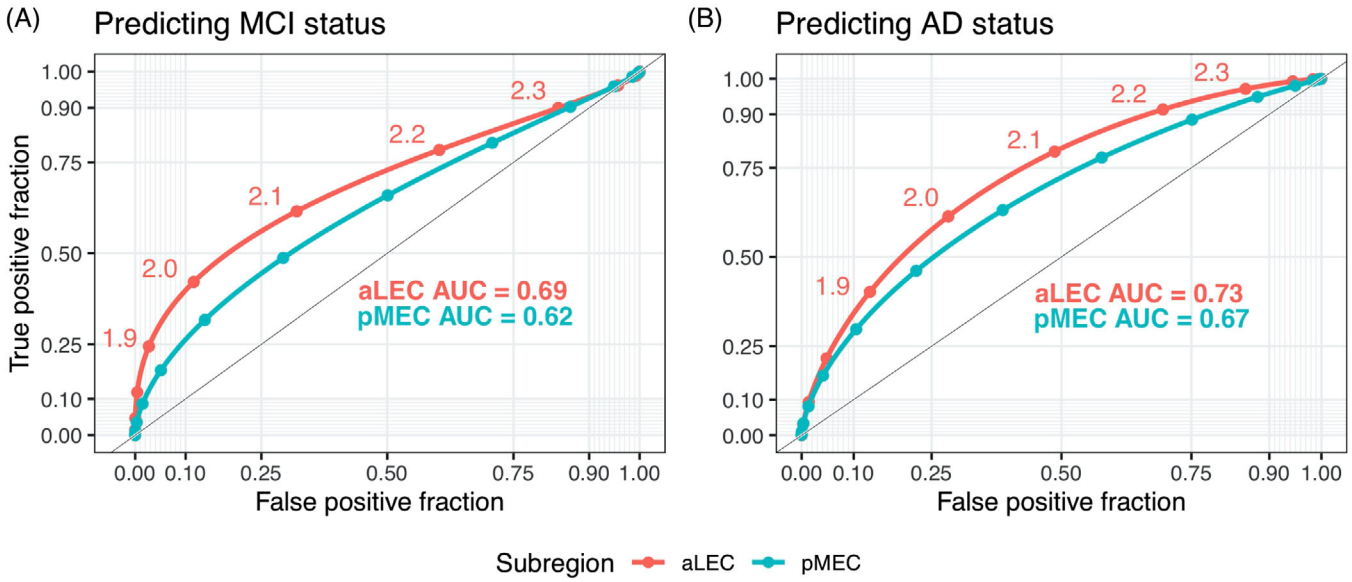

FIGURE 4 Receiver operating characteristic (ROC) curves for the prediction of mild cognitive impairment (MCI) status and AD status using anterolateral EC (ALEC) and posteromedial entorhinal (pMEC) cortical thicknesses (CT). A, In predicting MCI status, the aLEC curve dominates the respective pMEC curve and exhibits a larger area under the curve (area under these curves [AUC] 0.69 vs 0.62; with 95% confidence interval [CI; 0.066, 0.080] for difference). B, In predicting AD status, the aLEC curve also dominates the respective pMEC curve and exhibits a larger AUC (0.73 vs 0.67; with 95% CI [0.050, 0.064] for difference)

thinning may be an early marker that may be associated with cognitive decline especially in the memory domain and may serve as a mechanistic link between pathological load and cognitive outcomes. Additional research should focus on further understanding the function of aLEC and structural trajectories with aging and disease. For example, the human aLEC appears is involved in tasks ranging from visual object pattern separation[7,9] to intra-item configural processing[47] to temporal precision in real-world stimuli.[48] Developing tasks that are specific and sensitive to aLEC (dys)function could serve as an early predictor of cognitive decline. In the future, these tasks can provide measures that can be used as neurobiologically validated outcomes for clinical trials in preclinical AD.

ACKNOWLEDGMENTS

We acknowledge our sources of funding: T32 AG000096 (AH), NSF DGE-1321846, and B2D-1612490 (FM), as well NIA R01AG053555 and P50AG05146 (DG and MAY). We also acknowledge posthumously our co-author Jared Roberts who inspired and developed the initial stages of this project. Data collection and sharing for this project was funded by the Alzheimer's Disease Neuroimaging Initiative (ADNI; National Institutes of Health Grant U01 AG024904) and DOD ADNI (Department of Defense award number W81XWH-12-2-0012). ADNI is funded by the National Institute on Aging, the National Institute of Biomedical Imaging and Bioengineering, and through generous contributions from the following: AbbVie; Alzheimer's Association; Alzheimer's Drug Discovery Foundation; Araclon Biotech; BioClinica, Inc.; Biogen; Bristol-Myers Squibb Company; CereSpir, Inc.; Cogstate; Eisai Inc.; Elan Pharmaceuticals, Inc.; Eli Lilly and Company; EuroImmun; F. Hoffmann-La Roche Ltd and its affiliated company Genentech, Inc.; Fujirebio; GE Healthcare; IXICO Ltd.; Janssen Alzheimer Immunotherapy Research & Development, LLC; Johnson & Johnson Pharmaceutical Research & Development LLC; Lumosity; Lundbeck; Merck & Co., Inc.; Meso Scale Diagnostics, LLC; NeuroRx Research; Neurotrack Technologies; Novartis Pharmaceuticals Corporation; Pfizer Inc.; Piramal Imaging; Servier; Takeda Pharmaceutical Company; and Transition Therapeutics. The Canadian Institutes of Health Research is providing funds to support ADNI clinical sites in Canada. Private sector contributions are facilitated by the Foundation for the National Institutes of Health (www.fnih.org). The grantee organization is the Northern California Institute for Research and Education, and the study is coordinated by the Alzheimer's Therapeutic Research Institute at the University of Southern California. ADNI data are disseminated by the Laboratory for Neuro Imaging at the University of Southern California.

CONFLICTS OF INTEREST

The authors declare no conflicts of interest relevant to this article.

REFERENCES

1. Hyman BT, Van Hoesen GW, Damasio AR, Barnes CL. Alzheimer's disease: cell-specific pathology isolates the hippocampal formation. *Science*. 1984;225(4667):1168-1170.
2. Van Hoesen GW, Hyman BT, Damasio AR. Entorhinal cortex pathology in Alzheimer's disease. *Hippocampus*. 1991;1(1):1-8.
3. Braak H, Braak E. Demonstration of amyloid deposits and neurofibrillary changes in whole brain sections. *Brain Pathol*. 1991;1(3):213-216.

4. Gomez-Isla T, West HL, Rebeck GW, et al. Clinical and pathological correlates of apolipoprotein E epsilon 4 in Alzheimer's disease. *Ann Neurol*. 1996;39(1):62-70.
5. Kordower JH, Chu Y, Stebbins GT, et al. Loss and atrophy of layer II entorhinal cortex neurons in elderly people with mild cognitive impairment. *Ann Neurol*. 2001;49(2):202-213.
6. Price JL, Ko AI, Wade MJ, Tsou SK, McKeel DW, Morris JC. Neuron number in the entorhinal cortex and CA1 in preclinical Alzheimer disease. *Arch Neurol*. 2001;58(9):1395-1402.
7. Reagh ZM, Yassa MA. Object and spatial mnemonic interference differentially engage lateral and medial entorhinal cortex in humans. *Proc Natl Acad Sci U S A*. 2014;111(40):E4264-E4273.
8. Maass A, Berron D, Libby LA, Ranganath C, Düzel E. Functional subregions of the human entorhinal cortex. *Elife*. 2015;4(JUNE):1-20.
9. Reagh ZM, Noche JA, Tustison NJ, Delisle D, Murray EA, Yassa MA. Functional imbalance of anterolateral entorhinal cortex and hippocampal dentate/ca3 underlies age-related object pattern separation deficits. *Neuron*. 2018;97(5):1187-1198.e4.
10. Olsen RK, Yeung L-K, Noly-Gandon A, et al. Human anterolateral entorhinal cortex volumes are associated with cognitive decline in aging prior to clinical diagnosis. *Neurobiol Aging*. 2017;57:195-205.
11. deToledo-Morrell L, Stoub TR, Bulgakova M, et al. MRI-derived entorhinal volume is a good predictor of conversion from MCI to AD. *Neurobiol Aging*. 2004;25(9):1197-1203.
12. Devanand DP, Pradhaban G, Liu X, et al. Hippocampal and entorhinal atrophy in mild cognitive impairment: prediction of Alzheimer disease. *Neurology*. 2007;68(11):828-836.
13. Jauhiainen AM, Pihlajamäki M, Tervo S, et al. Discriminating accuracy of medial temporal lobe volumetry and fMRI in mild cognitive impairment. *Hippocampus*. 2009;19(2):166-175.
14. Pennanen C, Kivipelto M, Tuomainen S, et al. Hippocampus and entorhinal cortex in mild cognitive impairment and early AD. *Neurobiol Aging*. 2004;25(3):303-310.
15. Weiner MW, Veitch DP, Aisen PS, et al. The Alzheimer's disease neuroimaging initiative: a review of papers published since its inception. *Alzheimer's Dement*. 2012;8(1):S1-S68.
16. Fischl B, Dale AM. Measuring the thickness of the human cerebral cortex from magnetic resonance images. *Proc Natl Acad Sci U S A*. 2000;97(20):11050-11055.
17. Holland D, Brewer JB, Hagler DJ, Fennema-Notestine C, Dale AM, Initiative ADN. Subregional neuroanatomical change as a biomarker for Alzheimer's disease. *Proc Natl Acad Sci U S A*. 2009;106(49):20954-20959.
18. Desikan RS, Cabral HJ, Settecase F, et al. Automated MRI measures predict progression to Alzheimer's disease. *Neurobiol Aging*. 2010;31(8):1364-1374.
19. Ewers M, Walsh C, Trojanowski JQ, et al. Prediction of conversion from mild cognitive impairment to Alzheimer's disease dementia based upon biomarkers and neuropsychological test performance. *Neurobiol Aging*. 2012;33(7):1203-1214.
20. Reuter M, Fischl B. Avoiding asymmetry-induced bias in longitudinal image processing. *Neuroimage*. 2011;57(1):19-21.
21. Yushkevich PA, Avants BB, Das SR, Pluta J, Altinay M, Craige C. Bias in estimation of hippocampal atrophy using deformation-based morphometry arises from asymmetric global normalization: an illustration in ADNI 3 T MRI data. *Neuroimage*. 2010;50(2):434-445.
22. Das SR, Avants BB, Grossman M, Gee JC. Registration based cortical thickness measurement. *Neuroimage*. 2009;45(3):867-879.
23. Wang H, Yushkevich PA. Multi-atlas segmentation with joint label fusion and corrective learning—an open source implementation. *Front Neuroinform*. 2013;7:27.
24. Yushkevich PA, Wang H, Pluta J, et al. Nearly automatic segmentation of hippocampal subfields in in vivo focal T2-weighted MRI. *Neuroimage*. 2010;53(4):1208-1224.
25. Avants BB, Tustison NJ, Song G, Cook PA, Klein A, Gee JC. A reproducible evaluation of ANTs similarity metric performance in brain image registration. *Neuroimage*. 2011;54(3):2033-2044.
26. Avants BB, Tustison NJ, Stauffer M, Song G, Wu B, Gee JC. The insight toolKit image registration framework. *Front Neuroinform*. 2014;8:44.
27. Tustison NJ, Holbrook AJ, Avants BB, et al. Longitudinal mapping of cortical thickness measurements: an Alzheimer's disease neuroimaging initiative-based Evaluation Study. *J Alzheimers Dis*. 2019;71(1):165-183.
28. Avants BB, Yushkevich P, Pluta J, et al. The optimal template effect in hippocampus studies of diseased populations. *Neuroimage*. 2010;49(3):2457-2466.
29. Tustison NJ, Avants BB. Explicit B-spline regularization in diffeomorphic image registration. *Front Neuroinform*. 2013;7:39.
30. Tustison NJ, Avants BB, Cook PA, et al. The ANTs cortical thickness processing pipeline. Proc. SPIE 8672, Medical Imaging 2013: Biomedical Applications in Molecular, Structural, and Functional Imaging, 86720K. 2013. https://doi.org/10.1117/12.2007128
31. Klein A, Ghosh SS, Bao FS, et al. Mindboggling morphometry of human brains. *PLoS Comput Biol*. 2017;13(2):e1005350.
32. Lehmann G, Legland D. Efficient N-Dimensional surface estimation using Crofton formula and run-length encoding. *Insight J*. 2012.
33. Verbeke G, Molenberghs G. *Linear Mixed Models for Longitudinal Data*. Berlin, Germany: Springer Science & Business Media; 2009.
34. Ruppert D, Wand MP, Carroll RJ. *Semiparametric Regression*. Cambridge: Cambridge University Press; 2003.
35. Huang HK. Evaluation of diagnostic systems: methods from signal detection theory by J. A. Swets and R. M. Pickett. *Med Phys*. 1983;10(2):266-267.
36. Harari O, Cruchaga C, Kauwe JSK, et al. Phosphorylated tau-Aβ42 ratio as a continuous trait for biomarker discovery for early-stage Alzheimer's disease in multiplex immunoassay panels of cerebrospinal fluid. *Biol Psychiatry*. 2014;75(9):723-731.
37. Fagan AM, Mintun MA, Mach RH, et al. Inverse relation between in vivo amyloid imaging load and cerebrospinal fluid Abeta42 in humans. *Ann Neurol*. 2006;59(3):512-519.
38. Fagan AM, Roe CM, Xiong C, Mintun MA, Morris JC, Holtzman DM. Cerebrospinal fluid tau/beta-amyloid(42) ratio as a prediction of cognitive decline in nondemented older adults. *Arch Neurol*. 2007;64(3):343-349.
39. Grill JD, Nuño MM, Gillen DL, Initiative ADN. Which MCI patients should be included in prodromal Alzheimer disease clinical trials? *Alzheimer Dis Assoc Disord*. 2019;33(2):104-112.
40. Team RC. An Introduction to R. Samurai Media Limited; 2015. https://books.google.com/books/about/An_Introduction_to_R.html?hl=&id=tGwdswEACAAJ%20LB-i5JN.
41. Heisterkamp H, Simon S, Heisterkamp H, et al. Update of the nlme package to allow a fixed standard deviation of the residual error. *RJ*. 2017;9(1):239-251.
42. Wickham H. Programming with ggplot2. *Use R!*. 2016:241-253.
43. Sachs MC. PlotROC: a tool for plotting ROC curves. *J Stat Softw*. 2017;79.
44. Holtzman DM, Goate A, Kelly J, Sperling R. Mapping the road forward in Alzheimer's disease. *Sci Transl Med*. 2011;3(114):114ps48-114ps48.
45. Buerger K, Ewers M, Pirttila T, et al. CSF phosphorylated tau protein correlates with neocortical neurofibrillary pathology in Alzheimer's disease. *Brain*. 2006;129(11):3035-3041.
46. Strozyk D, Blennow K, White LR, Launer LJ. CSF A 42 levels correlate with amyloid-neuropathology in a Population-Based Autopsy Study. *Neurology*. 2003;60(4):652-656.
47. Yeung L-K, Olsen RK, Bild-Enkin HEP, et al. Anterolateral entorhinal cortex volume predicted by altered intra-item configural processing. *J Neurosci*. 2017;37(22):5527-5538.

48. Montchal ME, Reagh ZM, Yassa MA. Precise temporal memories are supported by the lateral entorhinal cortex in humans. *Nat Neurosci*. 2019;22(2):284-288.
49. Petersen RC, Aisen PS, Beckett LA, et al. Alzheimer's Disease Neuroimaging Initiative (ADNI): clinical characterization. *Neurology*. 2010;74(3):201-209.
50. Jack Jr CR, Bernstein MA, Fox NC, et al. The Alzheimer's Disease Neuroimaging Initiative (ADNI): MRI methods. *J Magn Reson Imaging*. 2008;27(4):685-691.

SUPPORTING INFORMATION

Additional supporting information may be found online in the Supporting Information section at the end of the article.

How to cite this article: Holbrook AJ, Tustison NJ, Marquez F, et al. Anterolateral entorhinal cortex thickness as a new biomarker for early detection of Alzheimer's disease. *Alzheimer's Dement*. 2020;12:e12068. https://doi.org/10.1002/dad2.12068